TÉCNICO LISBOA

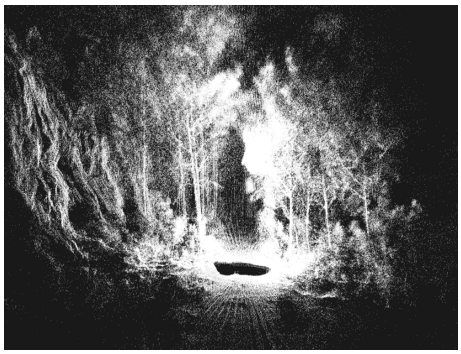

LiDAR data acquisition and processing for ecology application

Ion Ciobotari

Thesis to obtain the Master of Science Degree in

Electrical and Computer Engineering

Supervisor(s):
Prof. Doutor João Nuno de Oliveira e Silva
MSc. Adriana Príncipe da Silva

Examination Committee

Chairperson: Prof. Doutora Teresa Maria Sá Ferreira Vazão Vasques
Supervisor: Prof. Doutor João Nuno de Oliveira e Silva
Member of the Committee: Prof. Doutor Bruno João Nogueira Guerreiro

January 2021

Declaration

I declare that this document is an original work of my own authorship and that it fulfils all the requirements of the Code of Conduct and Good Practices of the Universidade de Lisboa.

Dedicated to my parents.

Acknowledgments

I would like to express my deepest gratitude to all of my supervisors Prof. João Oliveira and Adriana Silva and to Alexandra Silva, for giving me the opportunity to work on this topic under their supervision. This work would not have been possible without their guidance, knowledge, patience and time.

The author also thanks SECIL-Group for allowing access to their limestone quarry in Setúbal, Portugal, and João Gomes Mota and Albatroz Engenharia SA. for sharing their point cloud data.

Special appreciation go to my parents, who believed and supported me throughout this whole journey. Finally, I would like to thank all of my friends for always being there and keeping me company in both fun and tough times.

Resumo

A recolha de dados ecológicos no campo é essencial para diagnosticar, monitorizar e gerir os ecossistemas de forma sustentável. Contudo, a aquisição desta informação de forma tradicional é geralmente morosa, havendo a crescente tendência para a automatização da aquisição de dados através de sensores que registam um grande volume de dados em curtos períodos. Os laser scanners terrestes (TLS), em particular os sensores LiDAR, têm vindo a ser usados em ecologia, permitindo reconstruir a estrutura 3D da vegetação, e assim inferir características dos ecossistemas com base na variação espacial da densidade de pontos. Contudo, a baixa quantidade de informação obtida por feixe, a falta de ferramentas de análise de dados e a especialização das existentes, e o elevado custo dos equipamentos limitam a sua utilização. Neste trabalho desenvolveu-se um TLS de baixo-custo ($<$10k€) e mecanismos de aquisição e processamento de dados aplicáveis a dois casos de estudo: um parque urbano e uma zona alvo de restauro ecológico. A orientação do LiDAR foi modificada para realizar observações no plano vertical e foi integrado um motor para rotação do mesmo, possibilitando assim a aquisição de dados de 360° com elevada resolução. Foram ainda integrados sensores de movimento e localização para correção automática de erros e georreferenciação e desenvolvida uma aplicação para visualizar e analisar os resultados obtidos. Este sistema foi usado na análise de vários locais com estrutura da vegetação diferentes. Dos dados gerados pelo TLS em cada local, foram criados histogramas que caracterizam o número de pontos adquiridos por altura da vegetação, de onde foi fácil distinguir o estrato arbustivo do estrato arbóreo, tal como calcular a altura máxima de árvores e cobertura arbustiva. Estes resultados concordaram com os dados de campo, pelo que o TLS desenvolvido tem demonstrado ser eficaz no cálculo de métricas de complexidade estrutural da vegetação.

Palavras-chave: deteção remota, ecologia, LiDAR, sistema laser estacionário, low cost

Abstract

The collection of ecological data in the field is essential to diagnose, monitor and manage ecosystems in a sustainable way. However, the acquisition of this information through traditional methods are generally time-consuming, as such, there has been a growing trend towards automation of data acquisition through sensors that record a large volume of data in short periods of time. Terrestrial laser scanners (TLS), in particular LiDAR sensors, have been used in ecology, allowing to reconstruct the 3D structure of vegetation, and thus, infer ecosystem characteristics based on the spatial variation of the density of points. However, the low amount of information obtained per beam, the lack of tools for data analysis and specialisation of existing ones, and the high cost of the equipment limit their use. In this work, a low-cost TLS ($<$10k€) was developed along with data acquisition and processing mechanisms applicable in two case studies: an urban garden and a target area for ecological restoration. The orientation of LiDAR was modified to make observations in the vertical plane and a motor was integrated for its rotation, thus enabling the acquisition of 360° data with high resolution. Motion and location sensors were also integrated for automatic error correction and georeferencing and an application was developed to view and analyse the results obtained. From the data generated by the developed TLS, histograms of point density variation along the vegetation height were created, from where it was easy to distinguish the shrub stratum from the tree stratum, and maximum tree height and shrub cover were also calculated. These results agreed with the field data, whereby the developed TLS has proved to be effective in calculating metrics of structural complexity of vegetation.

Keywords: remote sensing, ecology, LiDAR, stationary laser scanning, low cost

Contents

List of Tables

List of Figures

Chapter 1

Introduction

Ecology is the science that studies the interaction between organisms and the biophysical environment they inhabit, including both biotic and abiotic components. Ecology studies require sampling field data, which demand intensive labour and time consumption for its collection. Therefore, methods and/or technologies, such as remote sensing, are bringing new opportunities to collect higher amounts of data with varying resolutions, but generally over areas which are paramount for ecology studies. Remote sensing, a noncontact technology, uses the reflected light by the area or target that is observed to make measurements of either location (and size) or nature of the target. Depending of the remote sensing system implementation, large study areas can be analysed and provide a larger amount of information than manual observation methods [1–3].

1.1 LiDAR and ecology

Remote sensing is a generalised term which can be expanded in different technologies and methods. From these technologies, this work focuses on Light Detection and Ranging (LiDAR) and its application in plant ecology. LiDAR is a laser light emission based technology which calculates the distance to an observed area or target. From acquired LiDAR data, also denoted as point clouds, 3D reconstruction of the surroundings of the sensor can be computed.

When applied in ecology, LiDAR shows great potential in acquiring large amount of information of vegetation structure which has been applied in various case studies, such as: collecting information to evaluate forest standard dendrometric parameters (i.e. stem diameters, tree height, stem density, basal area and commercial wood volumes), canopy characterisation (i.e. canopy cover and gap fraction, leaf area ratios and foliage distribution) and tree structure modelling [4–6], monitoring multiple ecological restoration objective outcomes [7], determination of carbon biomass production [8], and quantification of vegetation structure complexity using height diversity indices [9–11]. Vegetation structure is considered as a primary determinant of habitat quality, defining the distribution and abundance of critical habitat components for animals, such as food, nesting sites, shelter, cover against predation and camouflage [12].

1.2 LiDAR systems

There are many types of LiDAR systems, which can be generalised in three major platforms: spacial, aerial and ground systems. Beland et al. [13] characterised some of these systems in terms of area coverage, resolution and main area of occlusion. Area coverage refers to the typical spacial area that the system is able to capture, with consideration on the system mobility. Resolution refers to the level of detail resolved from LiDAR measurement, typically presented as the minimum distance between two points or as the minimum angle between laser firings. The lower these values are, the higher the resolution and detail of the point cloud. This characteristic is directly dependent on the size of the sensor footprint (the size of a laser sampling area) and spacing separating each footprint. Area coverage and resolution respectively increase and decrease with the distance from the sensor. Occlusion refers to blocking or shadowing of laser pulses by the target area of object, reducing the amount of information that can be extracted. By using these parameters to characterise LiDAR systems it's possible to discern their advantages and limitations. Doing so allows an user to choose the system best suited for his needs.

Space LiDAR systems (SLS), as the name suggests, are implemented on satellites. Being on orbit around the Earth, these systems have the greatest area coverage, almost global, with data being continuously acquired. However, they also have the greatest laser footprint, greatly reducing data resolution. Although aerial LiDAR systems (ALS) operate at much lower altitudes than SLS, they also have large footprints and low resolution. However, newer aerial models are implemented on drones, allowing data capture at lower heights, just above tree heights, reducing the footprint and increasing image resolution. This way, unmanned aerial LiDAR systems (UALS) provide better means to extract information from large areas and with better detail than ALS. Ground or terrestrial systems (TLS) have the lowest and greatest values in area coverage and resolution, respectively. This type of systems can be stationary or mobile. Mobile terrestrial systems (MLS), when compared with their stationary counterpart, are capable of greater area coverage. However, due to mobility, less time is spent on each visible target, reducing the system resolution, and are more prone for measurement errors. Occlusion of all of these systems depends not only on the system general location (ground, above ground, below and above canopy levels), but also on vegetation density of the study area. For example, in highly dense tree vegetation, using above canopy level systems, SLS, ALS and UALS, the main location of occlusion is present on the lower canopy of trees. For ground level systems, TLS and MLS, the main location of occlusion is present on the upper canopy of trees and at ground level, depending on height and density of shrubs.

1.3 Problem

Since the early use of LiDAR systems, new improvements keep surging, especially related to the increase of the maximum range, measurement resolution, accuracy, quantity and quality of information, by also measuring reflective intensity and/or colour values of the target. However, with this continuous growth, LiDAR systems become more complex to implement, difficult to use and expensive. Table 1.1 shows some market options for stationary TLS, which start at price of around 20000 $. Looking at the

main specifications of these system, price is conditioned by the system maximum range and resolution. This is proven by first comparing the resolution of Leica BLK360, Faro FOCUS^S 70 and Surphaser 100HSX, which have similar measuring range (50-70m). From these models, Surphaser 100HSX is the most expensive (90000$), due to having the best resolution of 0.001mm, followed by Faro FOCUS^S 70 (35000$), with 1mm, and finally by Leica BLK360 (18500$), with 4mm. Looking at the TLS models with similar resolution, such as Leica BLK360, Maptek SR3 and Riegl VZ-400i, their differentiating factor is their maximum range. Starting with the most expensive model, Riegl Vz-400i (120000$), which also has the highest measuring distance of 800m, followed by Maptek SR3 (50000$), with measuring distance of 600m, and finally Leica BLK360 (18500$), with a measuring distance of 60m.

An alternative to these systems is to develop the desired system using commercially available LiDAR sensor. However, these LiDAR sensors possess limited field of view, usually capturing only horizontal planes, lower accuracy and/or resolution. Accuracy may prove difficult to improve, since it's characteristic of the LiDAR sensor model, field of view and resolution can be improved with the use of additional components, however, depending on platform, implementation can be considered difficult and complex. For example, Zebedee [14] is a MLS composed of a laser scanner, acquiring data on a 2D plane, coupled to an inertial measurement unit (IMU) and attached to spring. With the developed of specialised algorithms and accurate estimation of the behaviour of the scanner during motion quality 3D point cloud were acquired. Although the hardware components of this system may seem simple, the overall implementation of this system may prove difficult and complex.

Table 1.1: Commercially available TLS and their specifications.

3D scanner	Price	Max. range	Field of view	Max. resolution	Scan speed
Leica Geosystems BLK360	18500$	60m	360°x300°	4mm	0.36M points/sec
Faro FOCUS^S 70	35000$	70m	360°x300°	1mm	1M points/sec
Maptek SR3	50000$	600m	360°x130°	4mm	0.2M points/sec
Surphaser 100HSX	90000$	50m	360°x270°	0.001mm	0.8M points/sec
Riegl VZ-400i	120000$	800m	360°x100°	5mm	0.5M points/sec

1.4 Outcomes

The main purpose of this work is to develop an easy to build and reliable TLS. This system must be low cost, capable of capturing point clouds with height precision and resolution. This thesis presents the architecture and implementation of such system, which is mainly composed by changing the LiDAR sensor visual orientation and, with the help of supporting components, to both increase its resolution and to achieve the desired field of view. This solution's total cost did not exceed a value of 10000€, lower than the cheapest TLS presented previously. The developed system was also tested in various environments, where it showed great point cloud detail and measurements with resolution equivalent to LiDAR systems with a price of 20000€. Since the developed system showed promising results, there

may be potential for the implementation of a similar system using much cheaper LiDAR sensors, further lowering the system cost and increasing application of this technology.

This work was presented at the scientific meeting, XIX National Ecology Meeting organised by SPECO (Portuguese Ecology Society). In a short presentation, with a duration of around 5 minutes, was possible to present how this system was implemented and its results in determining some environmental characteristics. The certificate of participation in this meeting is in annex A.

1.5 Thesis outline

Chapter 1 serves as a brief introduction and motivation for the use of LiDAR technology in ecology studies. In particular, present the main platforms of LiDAR systems, their advantages and disadvantages and their most common ecological application. Chapter 2 can be separated in two parts. The first part focuses on the usability of some remote sensing solutions, their application in ecology and limitations compared with the use of LiDAR. Next, in the second part, it's made an analysis on LiDAR sensor measurement methods and characteristics, mainly market price, maximum distance, data generation and communication interface, and point cloud data processing software. In chapter 3 the developed system is presented, along with eventual limitations of the system and possible solution. In chapter 4 is discussed the results acquired from the application of the developed system in different types of vegetation structures and in comparison with a mobile terrestrial system (MLS). Finally, chapter 5 summarises the main conclusions of this work and possible improvements and implementations for future research.

Chapter 2

Related work

2.1 Remote sensing

Remote sensing is the concept of data acquisition and processing of physical characteristics of distant objects. Data acquisition is usually done in the form of pictures through sensors capable of detecting electromagnetic energy, such as radio, visible light, infrared and ultra-violet. Data processing is the transformation of raw acquired data into usable information for the user. Depending on the method of data acquisition, remote sensing technologies can be classified by one of two types: passive and active remote sensing.

2.1.1 Passive remote sensing

Passive remote sensing acquires data based on the natural radiation emitted of reflected by the target. Sunlight is the most common source of reflection measured by these systems.

Photogrammetry [15] is an example of passive remote sensing. This technology encompasses methods for data acquisition from photographic images. From the acquired data it's possible to obtain detailed 2D or 3D models of physical objects or environments. These models are obtained identifying and coupling together points common on the various photographic images that compose the data set. To identify these common points, for each captured image it's important to know camera location, angle and characteristics (the intrinsic parameters, such as lens distortion, focal length and pixel size).

Spectral imaging [16], which is another example of passive remote sensing, provides the wavelength distribution of a target object or area. These measurements are made by filtering the reflective signal of the target though various spectral bands. From these captured images it's possible to detect what type of material the target is composed of, or even completely identify the detected object.

2.1.2 Active remote sensing

Active remote sensing systems acquire data by emitting their own type of radiation, i.e. radio or infrared electromagnetic domains, towards a known direction and record its reflection. By calculating the time

between emission and detection of the signal's reflection, it's possible to determine location, speed, and direction of the target.

Two types of such technology is LiDAR and Radio Detection And Ranging (RADAR). Both work in similar fashion, differentiated by the type and wavelength of the emitted signal. While LiDAR emits infrared type laser pulses, with wavelength between 250 nm and 11 μm, RADAR emits microwaves or radio, with wavelengths between 1 mm and 10000 km. The low wavelength value of LiDAR instruments allows for more detailed description of the target structure. However, its signal is limited in range and susceptible to weather conditions, such as clouds, fog and rain. In case of RADAR, its signal suffers less absorption when contacting the target, proving a much larger detection range. RADAR is also mush less affected by weather conditions, however, it cannot provide the same level of target detail as its LiDAR counterpart.

2.1.3 Remote sensing applied to ecology

Information provided by spectral imaging can be used for target/anomaly detection and scene characterisation [16]. When applied in ecology, it allows for identification and mapping of vegetation types or even species [17, 18].

Photogrammetry is another technology that also allows creation of 3D environmental reconstructions. A large quantity of information can be extracted from these reconstruction, same as LiDAR. However, this technology can't extract information from the interior of vegetation. Gil et al. [19] compared a LiDAR and photogrammetry systems on creating a digital terrain model (DTM). In this study it was concluded that, in environments with more complex vegetation, photogrammetry systems provided less accurate DTMs, which was caused from reduced ground visibility. This way, LiDAR shows to be a more recommended approach to study more complex vegetation strctures, where there are shrubs and trees of different shapes and sizes.

As shown previously, LiDAR is a remote sensing technology with a multitude of applications. This is due to it's highly accurate measurements, from which detailed 3D environmental reconstructions can be made. Although this information only represents physical characteristics, by analysing the geometry of detectable objects more information can be extracted, further increasing the environment characterisation. In forest ecology, these objects can be classified as trees and from their geometrical characterisation it's possible to extract vegetation structure, such as height, diameter at breast height (DBH) and biomass, and structural diversity indices, used to measure vegetation complexity [9, 10].

RADAR is very similar do LiDAR, also providing distance measurements to a target, however, due to it's low resolution and precision, it's not as highly used. Sexton et al. [20] compared LiDAR, RADAR and field measurements on measuring tree canopy heights. From his work, due to its low cost, field measurements proved to be the best method for studying individual or small number of tree. In comparison, remote sensing provided an economically efficient way of acquiring information from a larger area. In his analysing of the information acquired by both LiDAR and RADAR, LiDAR presented the best result due to its finer precision.

2.2 LiDAR

2.2.1 Technology

LiDAR laser pulses have wavelength between 250 nm and 11 μm, belonging to the visible and near infrared electromagnetic spectrum. These pulses are rapidly emitted, up to 1500000 pulses per second, and by measuring the delay between emission and detection of each pulse, in combination with the constant light speed (3^8 m/s), the distance to the target is calculated (Figure 2.1). Based on the energy of each emitted pulse, this sensor can be also classified as micropulse or high-energy. Micropulse lasers are low powered and are classified as "eye-safe".

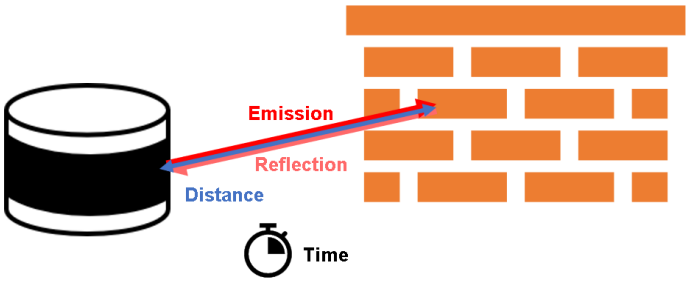

Figure 2.1: Conceptual representation of LiDAR sensor measuring method.

Furthermore, the LiDAR sensor is generally separated in two classes according to its range measurement method: full waveform and discrete returns [21] (Figure 2.2). Full waveform LiDAR returns an entire time-varying amplitude distribution of the directed laser focus. Discrete return LiDAR returns a static number of amplitude measurement. Each return is registered when the reflected signal exceeds a threshold. From these two measurement methods, discrete returns is the most commonly used, since it's easier to implement and returned data is easier to interpret.

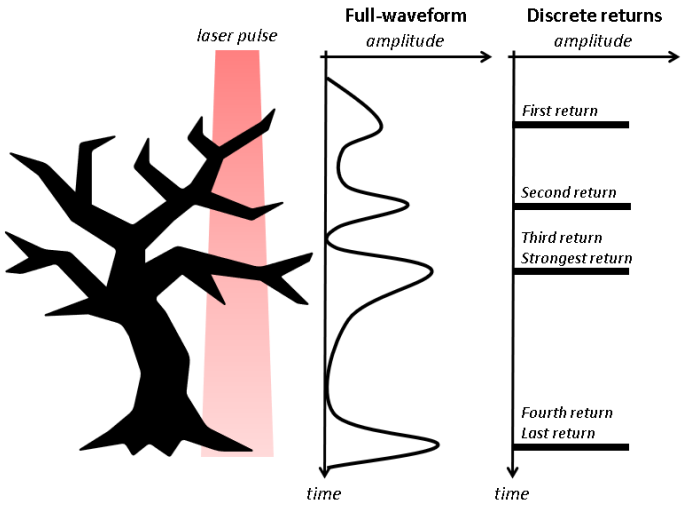

Figure 2.2: Conceptual difference between full waveform and discrete return LiDAR, with discrete return generating 4 measurements per pulse.

With development of new LiDAR sensors, in order to increase field of view and quantity of information, sensors started employing laser ”housing” [22]. This consists in pairing various lasers (Figure 2.3), which rapidly spins to scan the surrounding environment. Besides distance measurements, some LiDAR sensors also provide remission values, also called intensity and reflectivity. These values indicate how reflective is the target surface, which can be used to further increase target characterisation.

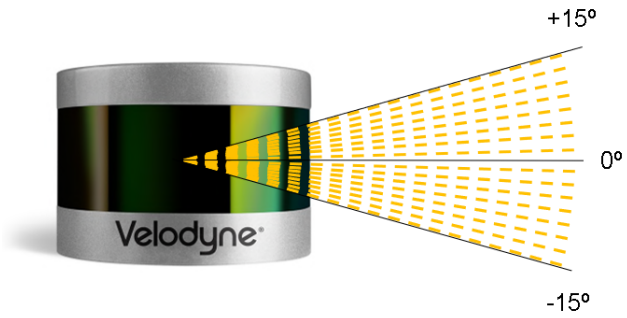

Figure 2.3: Representation of laser ”housing” of Velodyne VLP-16 LiDAR sensor model, composed of 16 laser with aperture of 2º.

2.2.2 Commercial product

In this section is presented and compared the specification of various commercially available LiDAR sensors. Table 2.1 provides the sensor measurement characteristics, such as maximum range , field of view and accuracy and resolution of both. Table 2.2 presents sensor price and processing characteristics, including sample rate (number of generated points per second), communication interface (channel from which user can read sensor data), number of discrete returns, number of channels (number of lasers coupled in laser ”housing”) and laser wavelength.

Looking at the Table 2.1, high-end sensors have an advantage in detection range and vertical field of view. However, this field of view is still very limited, where variation of the sensor plane of view is required for the user to extract more information about the surroundings. From the Table 2.2, it's possible to conclude that the number of available return measurements greatly increases the price of LiDAR sensors. This can be confirmed by comparing ibeo Lux sensors model characteristics, from both 2.1 and 2.2 tables, with other available high-end sensors, where the latter has inferior range, field of view and accuracy. This is expected, since increasing the number of returns requires greater analysis of reflected wavelengths, increasing the system complexity.

For ecology studies, range is an important factor when choosing the LiDAR sensor to use. In environments such as *dehesa*, also called *montado*, trees can reach height around 20m. In this kind of environment, short range LiDAR sensors, i. e. Slamtec RPLIDAR A3 and YDLIDAR G6 and G4 models from the Table 2.1, are inefficient. This way, usual off-the-shelf price of high-end LiDAR start at values above 1000$ (i.e. robosense RS-RUBY and OUSTER OS1-16), with some even reaching values above 50000$ (i.e. Velodyne HDL-64E). Nevertheless, LiDAR systems would make use of motion and rotation

mechanisms to increase the amount of obtainable information, further increasing system cost.

Standard use of LiDAR sensors makes acquisitions of horizontal images. The data extracted comes with two or three values for each point: azimuth angle, distance and intensity (some sensors do not provide this value). Using the azimuth and distance values, 2D point coordinates can be computed. If the sensor has laser ”housing”, by knowing the vertical field of view and aperture between lasers, 3D point coordinates can be computed. Depending on type of communication interface the sensors provides, data can easily be stored.

Table 2.1: LiDAR measurement characteristics.

Model	Max range	Accuracy [mm]	Resolution [mm]	Field of view (HxV)	Angular accuracy (HxV)	Angular resolution (HxV)
Velodyne						
HDL-64E	120	20	–	360°x26.9°	–	0.35°x0.4°
HDL-32E	100	20	–	360°x41.3°	–	0.4°x1.33°
VLP-16	100	30	–	360°x30°	–	0.4°x2°
ibeo						
Lux	50	100	40	110°x3.2°	0.25°x0.8°	–
SICK						
LD-MRS400001	300	100	40	110°x3.2°	0.125°	–
LMS111	20	12	–	270°	0.25°	–
MRS1104C	64	30	–	275°x7.5°	0.25°	–
OUSTER						
OS1-16	120	–	30	360°x33.2°	0.01°x0.01°	–
OS1-128	120	–	30	260°x45°	0.01°x0.01°	–
Surestar						
R-FANS16	200	20	–	360°x30°	–	0.36°
R-FANS-32	200	20	–	110°x28°	–	0.1°
C-FANS-128	200	20	–	360°x40°	–	0.1°
robosense						
RS-RUBY	200	30	–	360°x40°	–	0.1°
RS-LiDAR-32	200	30	–	360°x40°	–	0.4°x0.33°
Slamtec						
RPLIDAR A3	25	–	–	360°	0.225°	–
YDLIDAR						
G6	25	–	5	360°	0.28°	–
G4	16	–	5	360°	0.28°	–
SCANSE						
sweep v1.0	40	–	10	360°x0.5°	–	–

Table 2.2: LiDAR laser and processing characteristics.

Model	Price [$]	Sample rate [points/sec]	Comm. interface	Num. returns	Num. channels	Wavelength [nm]
Velodyne						
HDL-64E	>50000	1.3 M single/2.2 M dual	Eth	2	64	903
HDL-32E	>1000	695 k single/ 1.39 M dual	Eth	2	32	903
VLP-16	>1000	300 k single / 600 k dual	Eth	2	16	903
ibeo						
Lux	>10000	–	Eth, CAN	3	4 - 8	905
SICK						
LD-MRS400001	–	–	Eth, CAN	3	4	class 1[1]
LMS111	–	–	Eth, CAN, Serial	2	1	905
MRS1104C	–	–	Eth	3	4	820
OUSTER						
OS1-16	3500	327680	Eth	1	16	850
OS1-128	>1000	2621440	Eth	1	128	850
Surestar						
R-FANS16	–	320000	Eth, Serial	1	16	905
R-FANS-32	–	640000	Eth, Serial	1	32	905
C-FANS-128	–	640000	Eth, Serial	1	128	905
robosense						
RS-RUBY	>1000	2304000	Eth	2	128	905
RS-LiDAR-32	–	600 k single/1.2 M dual	Eth	1	32	905
Slamtec						
RPLIDAR A3	<1000	16000	UART	1	1	785
YDLIDAR						
G6	<1000	18000	USB, PH2.0-5P	1	1	785
G4	<500	9000	USB, PH2.0-5P	1	1	785
SCANSE						
sweep v1.0	<500	1075	UART, USB	1	1	class 1[1]

[1] eye-safe laser

2.2.3 Point cloud data formats

There are various LiDAR sensor models, each producing data in multiple formats. As previously seen, high-end sensors commonly provide raw data in UDP packet format, using Ethernet communication interface, which can be saved in pcap file format. Data structure of these packets, usually containing distance measurements, is specific to each manufacturer and hard for the user to directly interpret. This

way, it's necessary to convert raw LiDAR data into friendlier format. This data can also be used for processing, where more information can be inferred, i.e. classify each point has ground or non ground and assign it a colour code for future classification, filtering and/or visualisation. Some common point cloud file formats are:

- **txt/xyz:** non standardised ASCII file format based on representing xyz coordinates in lines of text. Although this type of file is widely compatible across programs, the lack of standardisation and specifications makes it slow to read and memory inefficient for big point clouds.
- **obj:** common format for 3D graphic applications. This file format is a simple data format that only represents 3D geometry, such as point coordinates, its colour and texture.
- **las:** binary format widely used and regarded as industry standard in representing LiDAR data. This file format can also store geographical references, various point attributes, such as xyz coordinates, reflective value, colour, classification, return number, and even attribute information on the LiDAR survey, i.e. for ALS it's possible to store flight date and time.

2.2.4 Point cloud processing software

With the evolution of LiDAR sensors, new software has been developed to improve LiDAR data acquisition and analysis. Data acquisition software is specific to the platform at which the LiDAR sensor is implemented and the model of the sensor itself. Data analysis software is developed according to the needs of the system operators. The geospatial open source community has worked on developing such software along with the definition of standard LiDAR data open formats and creation of algorithms and tools for accessing the processing such information. The Open Geospatial Consortium, an international consortium composed of various businesses, government agencies, research organisations and universities, has a dedicated working group actively discussing encoding, optimisation, processing and sharing point cloud data [23]. Some of the most common used tools and libraries are the following:

- **LAStools** [24]: "hybrid" software, in the sense that some modules are fully open source while others are free with point limitation (up to 15 million points depending on the module). When point limitation is exceeded, random noise is added, i. e., points are shifted in space randomly and some pixels may be turned to black. This tools allows data visualisation and classification (ground, non-ground, building and high vegetation, i.e. trees) and compute digital elevation models (DEM) and canopy metrics (i.e. heights, averages and standard deviation). Even though this tool uses highly efficient algorithms, its development was specialised for data acquired by aerial systems;
- **FUSION/LDV** [25]: software for visualisation and analysis of LiDAR data mainly for forestry applications. This tools allows the creation of surface and canopy models and sub plots, which can be used to individualise trees. When looking at sub plots containing trees the operator is also capable to measuring some of its attributes. The operator is also capable of measuring plot field statistics, i.e. height variations;

- **ArcGIS** [26]: software application for visualisation and manipulation of geographic information. This application allows an operator to create maps and add descriptive attributes. In forestry studies, this allows to classify terrain according to species, inventory, density, soil type and class/stand structure. Doing so allows an operator to monitor inventory of forest resources, damage from pests and timber harvesting [27];

- **TreeQSM** [28]: Matlab library that provides a modelling method that allows reconstruction of the woody structure of trees through 3D quantitative structure models. This reconstruction provides the operator the tree architecture, from which number of branches, length and diameter can be extracted. Data for this method must be a point cloud containing one single tree;

- **lidR**[29, 30]: comprehensive R package for aerial LiDAR data visualisation and computation of metrics for forestry applications. This package allows the calculation of point density (points/m^2) for total plot area, divide the plot area in grid cells and calculate point density of each cell and create a graphical representation of the results, calculate number of trees, tree heights and tree average height, and create histogram of points height to ground. It also contains functions for classification of ground returns, digital terrain model reconstruction, among many other applications;

- **Point Cloud Library (PCL)** [31]: open source software for visualisation and manipulation of point cloud data. This software features various algorithms for filtering, feature estimation, surface reconstruction and model fitting. Although not very appropriate for ecology studies, the algorithms can be used to segment relevant parts of a scene, extract key points and compute descriptors useful for object detection based on its geometry.

Although many point cloud data analysis tools exist, in ecology studies some tools may not provide enough functionality for environment characterisation. Likewise, tools and algorithms that provide such characterisation are usually specific to certain platforms, which may provide incorrect results when applied to point cloud data acquired by a different platform. This way, operators are left to develop their own methods to extract the information they require.

Chapter 3

Low cost LiDAR system (LCLS)

3.1 Objectives

This chapter describes the minimal architecture and implementation of a stationary terrestrial LiDAR system and complementary features for automatic image correction. The LiDAR sensor is the core of the system and the remaining components are responsible to increase the amount of data the it can acquire. This is achieved by increasing its field of view and resolution, and quality of the resulting point cloud, accomplished by transforming point coordinate according to system global position, terrain slope and compass orientation during the data capture. This system must be implemented using low cost components available on the market, with a total price below 10000€, and have enough accuracy and resolution for reliable application in ecology studies. The generated data must also be easily processed in order to compute metrics that the user deems necessary.

3.2 Requirements

From the applications presented in the previous chapters, the developed system is intended for ecological studies, specifically to monitor forest restoration. In order to justify the implementation and usage of this system some requirements must be met:

1 **High accuracy and resolution:** data acquisition must be done with high accuracy LiDAR sensors (i.e. Velodyne VLP-16, which has an accuracy of 3cm) and increase its resolution for the best measurements to create the best 3D reconstruction possible;

2 **Digital modelling of vegetation:** from the data acquired, a 3D digital model of the vegetation must be created for user visualisation and processing of its characteristics. This reconstruction must be georeferenced, north oriented and include a 360°x360°field of view of the captured environment. It's also important to ensure data quality in order to produce digital terrain models (DTM) of the analysed environment;

3 **Open data format:** data must have an adequate format type for easy reading and conversion between file format;

4 **Provide useful data:** besides space representation, it's important to allow the user to compute environment characterisation, quantify vegetation structure (i.e. height distribution of leaf density, height diversity indices and proxies of average height of trees and shrubs);

5 **Low cost:** the system must integrate a top-off-the-shelf LiDAR sensor and other used components must be easily obtainable in the market or man made to allow easy replication of the system;

6 **Ease of use:** the implemented system must be easily mounted every time it's used. Additionally, have an easy integration of software and hardware components to favour replication.

3.3 Architecture

Excluding the LiDAR sensor, the system can be divided in four parts, the hardware components and actuators responsible to carry and change the position of the LiDAR sensor, the actuator control, sensor acquisition and processing. A turn table is a simple hardware solution, capable to hold the LiDAR sensor and rotates it in the horizontal plane with the use of a step motor, the acting actuator of this implementation. The step size and number of steps taken per rotation of the step motor can be configured in order to increase the data acquisition and resolution in the horizontal plane. Besides the LiDAR sensor, this table can also be used to mount additional sensors deemed necessary to increase image quality or correction. Data acquisition of these sensors are used to verify the behaviour of the step motor and correction of the LiDAR data.

The LiDAR sensor provides the most part of sensor reading, more specifically, distance measurements to targets. The rest of sensor block is composed of location and movement tracking sensors. The actuators are responsible for moving the LiDAR sensor according to the instructions provided by the processing unit. This unit generates new instructions according to assessments of the data provided by the sensor block. As an example, whenever the sensor block acquires all measurements of a 2D vertical plane of its current position, sensor location, view orientation and terrain slope, the processing unit sends new instructions to the actuators in order to change the LiDAR to a new position for further data acquisition. Each 2D vertical plane data corresponds to all distance measurements produced by the LiDAR sensor equal to the number of samples of 360° vertical rotation it performs. Whenever data is acquired, it's immediately stored, minimising the delay between acquisitions. Afterwards, when data acquisition is finished, processing starts. During this time, the format of acquired data is validated and then used to compute a point cloud of the surrounding environment. Finally, through a User Interface (UI), the result is presented to the user.

Figure 3.1 shows the relationship between the various components that make the system. The support unit is composed by all hardware components used to complement the LiDAR sensor behaviour and data processing. The processing unit is responsible for all software functionalities, including data acquisition, aggregation and processing. The actuator is mainly composed of motors, used only for

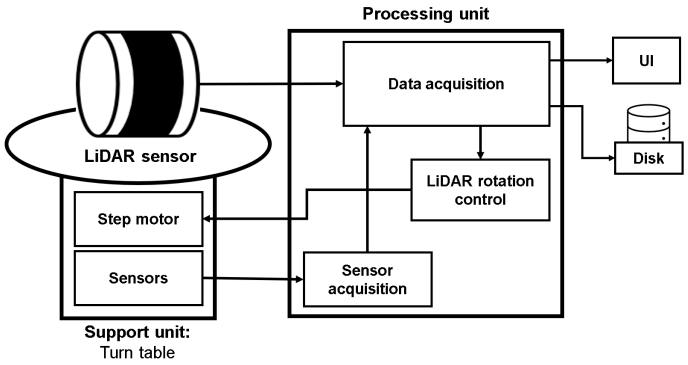

Figure 3.1: Block diagram of the system with explicit connections between its various components.

LiDAR sensor movement. The sensor block presents examples of available options which can measure location, i.e. Global Positioning System (GPS), or can derive movement information, i.e. gyroscope and accelerometer. Inside the processing unit are various blocks, each with very specific functions. The sensor acquisition block is responsible for acquiring data from all sensors (except LiDAR). Afterwards, this information is sent to data aggregation. This block couples LiDAR data with the previously mentioned sensor data in accordance to the LiDAR position and stores it in disk. During data acquisition, the data processing unit manages the number of samples (number of 360° vertical rotations) required for each vertical plane and creates new instructions to be sent to the motor controller. When data acquisition is finished, the data processing unit is responsible for point cloud computation and send the results to the UI. Finally, the motor controller is responsible for managing the system movement and rotation of the LiDAR sensor, according the instruction from the processing unit.

3.4 Implementation

3.4.1 LiDAR sensor

The LiDAR sensor model chosen for this system implementation is the VLP-16 (also called Puck) model from Velodyne (sensor specifications are present in Table 3.1). This sensor makes 16 simultaneous laser emissions on the horizontal plane with an aperture angle of 2°, for a field of view of 360°x30°, and up to 2 distance measurements per laser emission, ranging between 0.5m and 100m with an accuracy of 3cm (Tables 2.1 and 2.2). This sensor is mounted in a non conventional position, in order to capture the vertical plane instead of the typical horizontal plane (Figure 3.2). With this change, the field of view and angular resolution of the sensor are switched. This way, the sensor has a field of view of 30°x360° and an angular resolution in the horizontal and vertical plane of 2° and between 0.1°-0.4°.

Table 3.1: Velodyne VLP-16 sensor specification.

Maximum range	100 m
Minimum range	0.5 m
Accuracy	+/- 3 cm (typical)
Field of view (horizontal)	360º
Field of view (vertical)	30º (-15º to 15º)
Angular resolution (horizontal)	0.1º - 0.4º
Angular resolution (vertical)	2º
Laser wavelength	903 nm
Number of laser channels	16
Rotation speed	5 - 20 rps
Maximum number of return	2 (Strongest and Last)
Operating voltage	9 - 32 V
Communication interface	Ethernet (UDP)

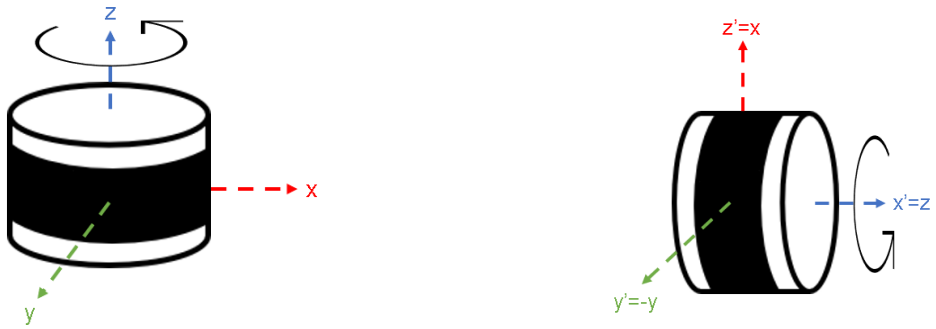

(a) (b)

Figure 3.2: (a) Standard orientation of the LiDAR sensor; (b) Proposed orientation of the LiDAR sensor

3.4.2 Hardware implementation for sensor rotation

The first objective of this stationary system is to achieve a spherical field of view (360°x360°), allowing for an increased data acquisition, such as detection of entire trees, its surrounding vegetation and ground terrain. To achieve this the LiDAR sensor is mounted on a turn table [32]. The step motor used to rotate the table is the Nema 17 model [33]. This motor is bipolar, in other words, it can rotate in both clockwise and counter-clockwise direction, and has a default step size of 1.8°. The system implementation using these components is presented on the Figure 3.3.

Depending on the motor step size, different levels of horizontal angular resolution can be achieved. Since the new orientation of the LiDAR sensor changed its horizontal resolution to 2°, with a step size of 1.8° and 0.9° the resulting system's horizontal angular resolution value is 0.2° and 0.1°, respectively. Through the configuration of the motor controller it's also possible to further decrease the step size improving horizontal resolution, however, doing so increases the difficulty to validate motor rotation and greatly increases the point cloud capture time.

Figure 3.3: Low Cost stationary LiDAR system. This system is composed by the LiDAR sensor (A), a turntable (B) and a step motor (C).

3.4.3 LiDAR rotation control

The motor is controlled by a combination of a step motor controller and additional sensors. The controller used is the Polulu Tic T500 [34] model. This controller allows the configuration of motor characteristics, such as rotation speed and acceleration, power consumption and step resolution. Step resolution defines a new step size the motor can perform. The model Tic T500 allows to configure the step size as full, half, 1/4 and 1/8 of the motor's default step size, which for the motor Nema 17 corresponds to 1.8°, 0.9°, 0.45° and 0.225°, respectively. The sensors used are LSM6DS3 [35] (accelerometer and gyroscope) and LSM303DLHC [36] (magnetometer). The accelerometer and gyroscope are used to complement validation of motor rotation and compute LiDAR tilt and the magnetometer to orient point cloud data to north. Figure 3.4 presents the electric connections between these components and with the processing unit.

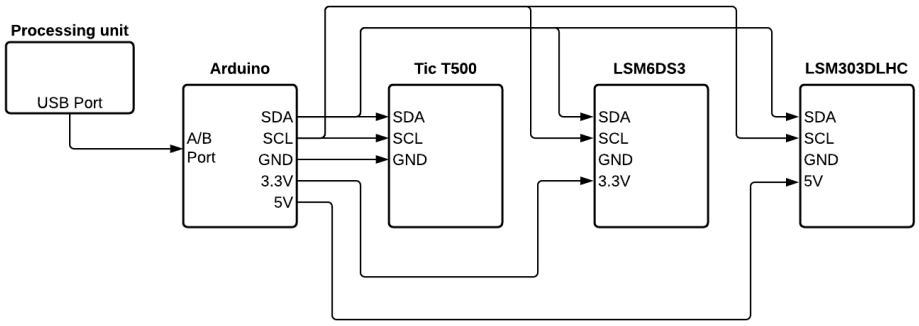

Figure 3.4: Electric connection between sensors and motor controller.

3.4.4 LiDAR tilt

Depending on the studied environment, terrain may not be uniform and, if the LiDAR sensor is not correctly levelled, the resulting point cloud presents an incorrect environment characterisation. To correct such behaviour, an inertial measurement unit (IMU) [35], composed of an accelerometer and gyroscope, is employed to automatically compute LiDAR tilt. The accelerometer provides the acceleration force in each directional axis and the gyroscope provides speed of angular rotation. Using these measurements, roll, pitch and yaw angles (3.5) can be computed using the expression 3.1, 3.2 and 3.3, based on the complementary filter implementation from [37]. In these expression, $Roll$, $Pitch$ and Yaw are the desired angles in degrees, Gx, Gy and Gz correspond to the gyroscope measurements, Ax, Ay and Az correspond to accelerometer measurements, T is the sampling period, including both sensor readings and angle calculations, and α is related to the time constant τ and the sampling rate through the expression 3.4. For the implementation of these sensors, the time constant was set to 0.1s.

$$Roll = \alpha \times (Roll_{prev} + Gx \times T) + (1 - \alpha) \times arctan\left(\frac{Ay}{Az}\right) \tag{3.1}$$

$$Pitch = \alpha \times (Pitch_{prev} + Gy \times T) + (1 - \alpha) \times arctan\left(\frac{-Ax}{\sqrt{Ay^2 + Az^2}}\right) \tag{3.2}$$

$$Yaw = Yaw_{prev} + Gy \times T \tag{3.3}$$

$$\alpha = \frac{\tau}{\tau + T} \tag{3.4}$$

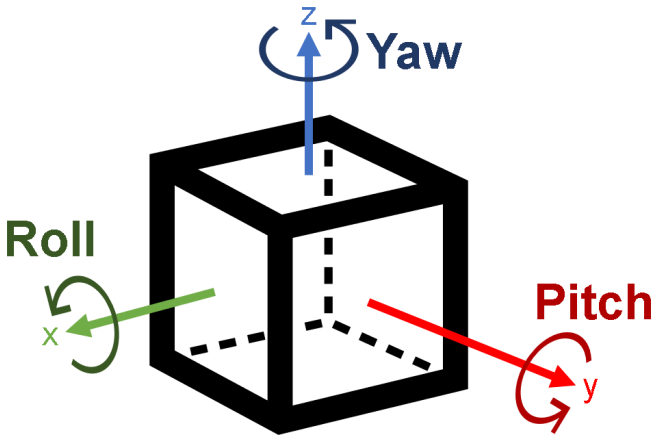

Figure 3.5: Graphical representation of an object 6 degrees of freedom (x, y and z axis and pitch, roll and yaw angles).

3.4.5 Data acquisition and processing

Data acquisition is done by two main components, Arduino UNO and a main processing unit, i.e. a laptop computer. The Arduino manages the behaviour of the motor controller, continuously updates sensor data and also works as a proxy between these components and the processing unit. This way, to change motor position, verify its status or get sensor data, first it's necessary to send the appropriate command to the Arduino, which interprets it and sends back a suitable response. For example, to change the motor position, the processing unit would send the corresponding command indicating the desired position and wait for a response. If the command was done successfully, the response contains the motor's new current position and an uncertainty code, indicating if the rotation was valid or not, otherwise, the processing unit receives an error message. When sending commands to acquire sensor data, if successful, the Arduino responds with the appropriate data. A simple representation of the Arduino workflow is present in the Figure 3.6.

The main processing unit reads all LiDAR data, both distance measurements and position provided by GPS, through Ethernet port and sensor data from Arduino. Afterwards, XYZ point coordinates are computed from LiDAR data and manipulated using the sensor data. From the block diagram in Figure 3.6, representing a point cloud capture workflow, to initialise a point cloud capture some user inputs are required: horizontal rotation (ROT), motor step size (STEP) and vertical plane sampling (REP). As the name suggests, horizontal rotation is referred as the maximum LiDAR sensor horizontal rotation and vertical plane sampling as number of samples of complete 360º LiDAR laser rotation per motor rotation. The initial position of the system is set according to the north orientation provided by the compass, if applicable, is set by current orientation of the LiDAR sensor. The rotation step corresponds to the number of motor steps taken between each vertical plane samplings.

When starting a point cloud capture, the first step is to compute LiDAR tilt. Afterwards, the processing unit reads LiDAR data corresponding to the total number of plane samples desired by the user. The sampled vertical plane is both stored it in a .txt file, in its raw format, and converted to XYZ point coordinate, along with its intensity value, I, and timestamp, T (time since the LiDAR sensor has been turned on). GPS is connected directly to the LiDAR sensor. Doing so improves the accuracy of timestamps of each measurement provided. This way, LiDAR becomes responsible of relaying to the processing unit the global position of the system. This data is never stored, since its only used once for point cloud georreferencing and ignored ever since. When data is stored, the processing unit sends new instructions to the actuator control to change to a new position. These two last steps, data reading and motor rotation, are repeated until the LiDAR sensor rotation corresponds to the user defined horizontal rotation. Finally, a point cloud is generated and available for user visualisation and further processing.

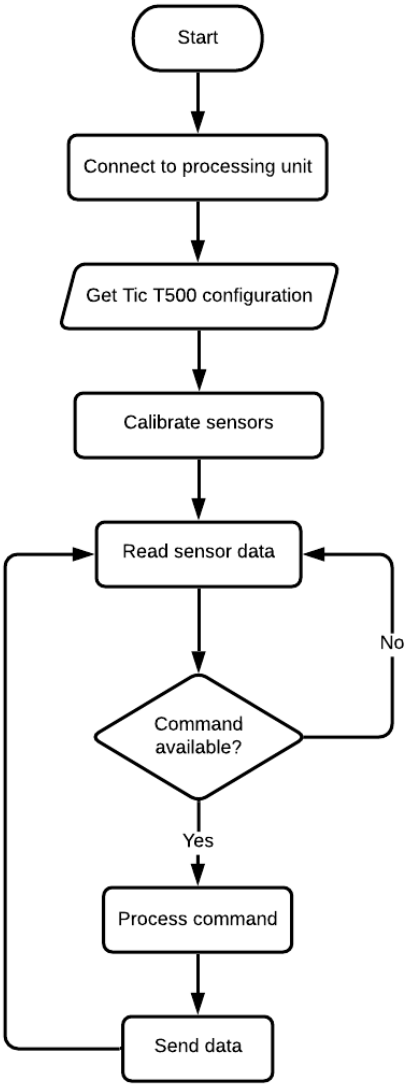

Figure 3.6: Block diagram representation of the Arduino general initialisation and behaviour.

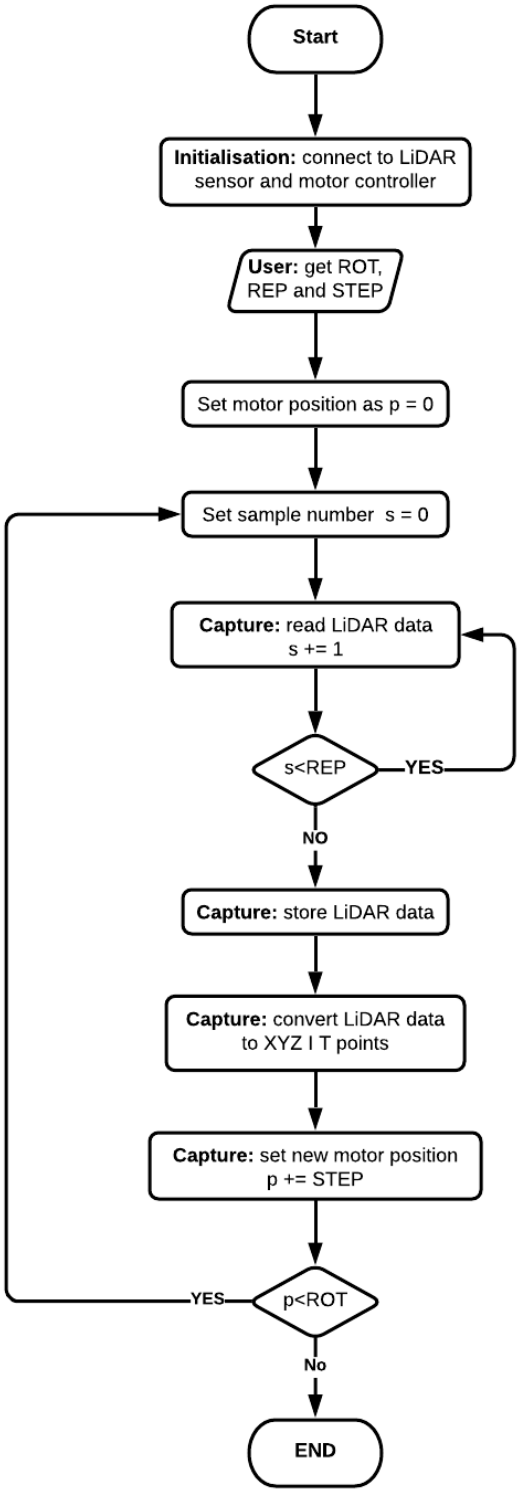

Figure 3.7: Block diagram representation of a LiDAR point cloud capture workflow. This workflow is specific for a LiDAR stationary system with horizontal rotation performed by a step motor and automatic point cloud correction.

Chapter 4

LCLS evaluation

4.1 Cost

Table 4.1 presents the main components for the system's implementation, along with their price and corresponding role, according to the architecture presented in the Figure 3.3.

Table 4.1: Components used for the LCLS implementation.

Component	Role	Price
Velodyne VLP-16	LiDAR sensor	11000€
Turntable	Support unit	49.75€
Tripod	Support unit	80€
Nema 17	Actuator	15.87€
Pololu Tic T500	Actuator controller	19.62€
Arduino Uno	Sensor acquisition	14.98€
LSM6DS3	Sensors	14.27€
LSM303DLHC	Sensors	9.59€
12V baterry	Support unit	13.95€
Total		11218.03€

The price of the LiDAR sensor VLP-16 model used was 11000€, above the price limit setup as requirements (10000€). This is due to the fact that the LiDAR sensor was bought in the year 2015. Since then, this model has had it's price decreased and many cheaper options with similar characteristics have appeared (see tables 2.1 and 2.2 for some examples of commercially available LiDAR sensors). The rest of the components proved to be easy to obtain with a total price below 600€, including some miscellaneous components, such as wires and bolts, and component shipment costs. This brings the total cost of the developed system below 11600€ and, since there are many cheaper options for the LiDAR sensor, the total cost can still be reduced.

4.2 Technical performance

4.2.1 Configuration and calibration

To keep the sampling process uniform, configuration and calibration of the different components used was equal for all study locations. The configuration of the step motor controller is present in the Table 4.2. The accelerometer and gyroscope were calibrated by computing their drift value, which corresponds to the mean value of multiple measurements with the sensor stationary in the starting position. The magnetometer measurements suffered no change since the model used comes factory calibrated.

Table 4.2: Pololu Tic T500 configuration used for step motor control.

Maximum speed	18000000 pulses/s
Starting speed	0 pulses/s
Maximum acceleration	20000 pulses/s
Maximum deceleration	20000 pulses/s
Step mode	full
Current limit	1452 mA
Decay mode[1]	Auto

[1] affects how fast the current flowing through the motor decays during each step

4.2.2 Distance assessment

Accuracy and resolution of the distance measurements were evaluated by computing multiple distances between various points. These distances were measured on site with a measurement tape and on the point cloud using CloudCompare [38] applications.

The study area used to evaluate these characteristics is the main hall of the central pavilion at Instituto Superior Técnico (IST) (38°44'12.8" N, 9°08'21.4" E), taken on 19 December 2020. The figures in 4.1 shows the various distances measured in the pavilion. Figure 4.2 presents a visualisation of the acquired point cloud data in this location.

The resulting measurements, both tape measured and from point cloud data, are presented in the Table 4.3. Both H and I are radial lines, beginning close to the LiDAR system and ending at maximum distances of 20-30m away. For this reason, distances from the LiDAR cannot be presented.

Looking at the results from the Table 4.3, distance measurements taken from point cloud were almost always underestimating field measurements. However, the difference between the two types of measurements is around 2cm, which, again, corresponds to the accuracy value in specifications (3.1) of the sensor used. This error is constant along with distance from the sensor. Distances H and I, which correspond to the largest distances measured, had a variation of 0.21m and -0.3m, respectively, from their field measurements, which can be explained by the lack of accuracy when tape measured.

Table 4.4 presents the minimum distance between two point cloud points at different distances of the position of the LiDAR sensor. The minimum distance directly provides the resolution value of the system according to the point cloud capture configuration. With a configuration of STEP 1, REP 10

(a) (b) (c) (d) (e) (f)

Figure 4.1: Central hall at IST with indication of all field measurements.

and ROT 180, the resolution varies with the distance to the LiDAR sensor. At short distances (5m) the resolution measured is around 0.042m (0.477°), higher than the value expected. This deviation is somewhat expected since this value is close to the measuring accuracy from the LiDAR specifications (3cm). At higher distances from the LiDAR (23m and 34m), the measured resolution are similar to the expected value. For a capture configuration with STEP 2, REP 5 and ROT 180, the behaviour of the results are similar to the previous configuration. Finally, together with accuracy results, it's safe to conclude that, for a stationary system, the LiDAR sensor is the main factor which dictates point cloud quality and measurement accuracy.

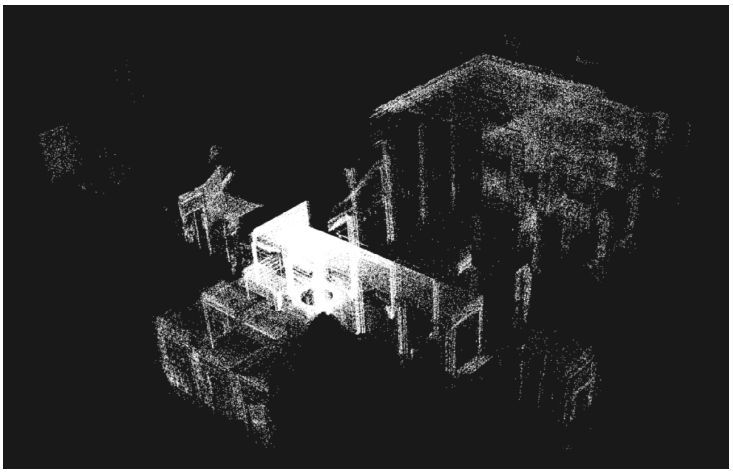

Figure 4.2: Point cloud data of the central hall at IST.

Table 4.3: Comparison of distance measurements taken from LiDAR point clouds and manually using a measuring tape.

Measurement ID	Distance from LiDAR [m]	Measurements		Error[1][m]	Error [%]
		Field [m]	LCLS [m]		
A	2.11	0.78	0.75	-0.03	-3.85
A	3.12	0.78	0.76	-0.02	-2.56
A	6.83	0.78	0.73	-0.05	-6.41
B	10.35	0.64	0.68	0.04	6.25
B	6.48	0.64	0.62	-0.02	-3.13
B	2.96	0.64	0.62	-0.02	-3.13
B	5.80	0.64	0.62	-0.02	-3.13
C	1.80	3.00	2.99	-0.01	-0.33
C	3.30	3.00	2.95	-0.05	-1.67
C	8.90	3.00	3.00	0.00	0.00
C	0.50	3.00	2.95	-0.05	-1.67
D	5.00	2.60	2.58	-0.02	-0.77
E	–	27.86	28.07	0.21	0.77
F	–	19.37	19.07	-0.3	-1.55

[1] LCLS - Field

Table 4.4: Horizontal resolution values from two different point cloud capture configuration at three distances from the sensor. Measured resolution corresponds to the average value of 10 samples.

STEP	REP	ROT	Angular resolution	Distance	Resolution	Measured resolution		
						Average		Standard deviation
1	10	180	0.2°	5m	0.0175m	0.0416m	0.477°	-0.0119
				23m	0.0803m	0.0887m	0.221°	0.0115
				34m	0.1187m	0.1185m	0.200°	0.0027
2	5	180	0.4°	5m	0.0349m	0.0539m	0.618°	0.0124
				23m	0.1606m	0.1725m	0.430°	0.0280
				34m	0.2373m	0.2270m	0.383°	-0.0316

4.3 Position sensors assessment

4.3.1 Tilt measurements

Accuracy of the LiDAR tilt measurements was performed by simulating angle variation, as shown in Figure 4.3, and by comparing roll and pitch angles provided by the sensor and manually measured using a protractor (minimum unit of 1°). In the Table 4.5 are the measured roll and pitch angles in three different situations: change in roll angle, change in pitch angle and change in both roll and pitch angles.

For each situation angles, three different angles were tested, between 11° and 37°, using the protractor. Changes in measured and sensed angles are below 3° in all combinations. Furthermore, for simulations of roll and pitch angles, sensor underestimated the measurements obtained with the protractor, which is concluded by the negative error values for roll angle and positive error values for pitch. For the variation of both roll and pitch, the error is positive for roll and negative for pitch, overestimating the protractor measurements. Overall, error variation is within acceptable margin this way, it can be concluded that the implementation of an accelerometer and gyroscope can be beneficial for the intended use of calculating terrain slope for correction of point cloud data. In addition, using more accurate expressions for calculating pitch, roll and yaw angles, or even improving calibration methods, may further reduce angle error.

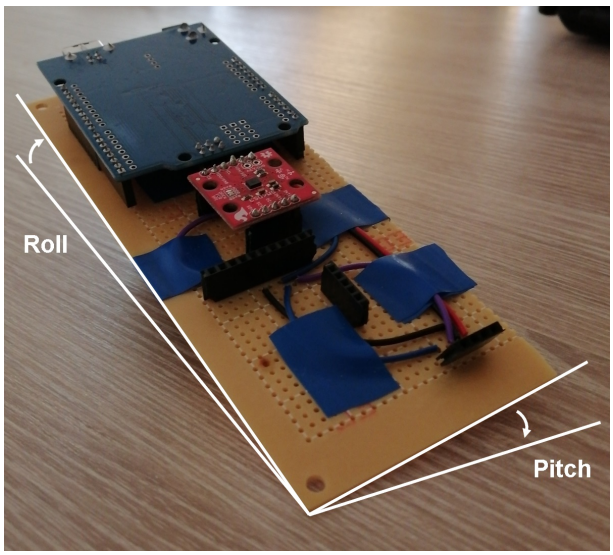

Figure 4.3: Developed Arduino shield.

4.3.2 Compass heading

The system's compass was implemented using a magnetometer, which provides a clockwise angle rotation to north. To test it's accuracy, the angle provided by the magnetometer was compared to measured angles provided by compass a application of a cellphone. Three angle measurements were tested, at 0°, 130° and 280° angles taken with the cellphone application. Results are shown in the Table 4.6 and indicate error increase with azimuth, with a minimum of 3.5° when north-oriented, increasing to 21° at

Table 4.5: Sensor angle measurements in three different situations.

Angles to test		Measurements		
		Field	Sensor	Error[1]
Roll		14°	13.76°	-0.24°
		24°	21.11°	-2.89°
		37°	34.85°	-2.15°
Pitch		-14°	-13.35°	0.65°
		-24°	-21.90°	2.01°
		-32°	-29.61°	2.39°
Roll and pitch	Roll	23°	20.44°	-2.56°
		15°	16.58°	1.58°
		31°	31.85°	0.85°
	Pitch	-11°	-11.30°	-0.3°
		-25°	-25.33°	-0.33°
		-20°	-21.92°	-1.98°

[1] Error calculated as Sensor - Field.

130° (corresponding to a 16% error) and to 34° at 280° rotation (corresponding to a 12%. This deviation between methods could have originated due to calibration from both the cellphone application and factory calibration of the magnetometer. Based on these preliminary results, no conclusion can be taken from the performance of this sensor for calculating angle difference with magnetic north and that further research is needed to account for these differences. A possible replacement for this sensor is to use compass heading computation methods based on gravity measurements [39], which can be acquired through accelerometers and gyroscopes.

Table 4.6: Measured angle difference with north.

Cellphone	Sensor	Error[1]	
280°	314.19°	34.19°	12.21%
0° (360°)	356.5°	-3.5°	-0.97%
130°	109.01°	-20.99 °	-16.15%

[1] Error calculated as Sensor - Manual.

4.3.3 Execution time and point cloud quality

Configuration of the LiDAR capture not only dictates the maximum horizontal resolution but also maximum number of points in the resulting point cloud and point cloud acquisition time. To evaluate these characteristics, multiple point clouds were generated with different capture configurations (5 point cloud samples per configuration) and execution time was measured. Number of points can be calculated using the expression 4.1, where NP is the number of points, $STEP$, REP and ROT correspond to the user required configuration, $mtSTEP$ is the step motor size in degrees and $vData$ is the number of points acquired per rotation. For VLP-16, the LiDAR sensor model used for the LCLS implementation, to acquire a 360° vertical plane, 82 UDP packets are needed and each provides 32 distance measurements, as such, $vData$ value for this model is $82 \times 32 = 2624$. The number of points calculated using this expression is equal to the number of points generated during point cloud capture.

$$NP = \frac{ROT}{STEP \times mtSTEP} \times REP \times vData \tag{4.1}$$

Looking at the results in the Table 4.7, execution time of acquisitions taken with ROT equal to 360° are double of acquisition taken with ROT equal to 180°. Increasing REP value also greatly increases the amount of points, dictated as number of points (REP=a) = a $\times$ number of points (REP=1), with very little increase in execution time, i.e. around 30s per REP value for STEP of 1 and ROT of 180°. Additionally, some configurations can be more efficient in point cloud acquisition than others. This can be observed by comparing the configurations REP 10 and ROT 180° with REP 5 and ROT 360°, using any STEP value for both configurations. Both configuration result in the same total number of acquired points and the former (REP 10 ROT 180°) has an execution time around half of the latter (REP 5 ROT 360°). This way, it's suggested that the ROT value is maintained at 180°, change STEP value according to the desired horizontal resolution and use REP to define the amount of points and detail of vertical planes of the resulting point cloud.

Table 4.7: Execution time and number of effective points acquired for various types of capture parameters.

STEP	REP	ROT	Execution time [min:s]	Number of points
1	1	180	8:46	262400
	5		10:19	1312000
	10		11:45	2624000
	1	360	17:27	524800
	5		20:07	2624000
	10		23:26	5248000
5	1	180	1:49	52480
	5		2:05	262400
	10		2:26	524800
	1	360	3:39	104960
	5		4:10	524800
	10		4:53	1049600

4.4 Measuring vegetation complexity

4.4.1 Case studies

The developed LCLS was used to capture point cloud data from two locations with very distinct types of vegetation structure. A first set of sampling were made at two urban gardens, at the park in Campo Grande (CG) (38°45'12.7" N, 9°09'04.0" W) and a garden at IST (PC) (38°44'15.4" N, 9°08'22.2" W). Both of these sites have similar type of vegetation, consisting of a small number of shrubs, which are often pruned, and trees that have similar shape and height. The second set of sampling was done in a limestone quarry (SECIL) (38°29'43.0" N, 8°57'02.5" W), where LiDAR captures were taken on four locations under ecological restoration, each with different age. Figure 4.4 shows the location of all sampling locations.

Figure 4.4: Location map of the sampled urban gardens and the different plots at the limestone quarry.

4.4.2 Data acquisition

Field sampling at the urban gardens in CG and PC consisted of measuring tree height and diameter at breast height DBH. For the sites at SECIL, a limestone quarry, shrub cover and height and tree density, height and DBH were measured by a research team from the Centre for Ecology, Evolution and Environmental Changes of the University of Lisbon. Shrub cover and height values were obtained by using a 2x10m line intercept method within a plot size of 10x10m. This method has been widely adopted to measure vegetation, consisting in extending a tape to create a transect across the site. The observer would then identify all plants intercepted by the tape and record each intercept distance, maximum height, and width. Cover is calculated by adding all measured shrub width and expressing this total as proportion of tape length [40]. Tree height and DBH were measured within a plot size of 10x20m. Tree height was measured using a Nikon Forestry Pro laser rangefinder.

For point cloud captures, the LCLS was mounted on a tripod and settled near the centre of each plot, whenever possible, with consideration of occlusion effects in order to increase environment characterisation within sampling plot. The configuration used for point cloud capture was STEP 1, REP 10 and ROT 180. SECIL1, SECIL2, SECIL3 and SECIL4 points clouds were taken on 20 of July 2020, PC point cloud was taken on 22 of July 2020 and CG was taken on 28 of July 2020.

CG and PC urban gardens share some characteristics, as they have low tree density, of 0.02 trees/m^2 and 0.006 trees/m^2, respectively. At these study sites, tree are quite tall, with maximum heights of 33.4m and 20.4m (Table 4.8). The plots at the limestone quarry are all different from the urban gardens, and also between themselves. SECIL2 and 4 develop on horizontal quarry platforms and are interrupted by a road that allows access to those revegetated areas of the quarry. SECIL 1 and 3 correspond to sloped surfaces developing on the side of the road. In these two cases, the LiDAR sensor could not be

positioned in the centre of the plot, but was instead placed in the middle of its lower long edge. SECIL 1, 2 and 4 have high tree density of 0.19 trees/m^2, 0.15 trees/m^2 and 0.09 trees/m^2. Tree size between these plots show averages of 8.5m, 10.8m and 12m. Furthermore, these plots are quite different in the shrub stratum development, as can be seen in shrub average height and total cover (Table 4.8). SECIL3 has no trees and only contains shrubes.

Figures 4.5, 4.6, 4.7, 4.8, 4.9 and 4.10 present the resulting visualisation of each acquired point clouds. These images were taken using visualisation functions from Python-PCL [41] library, a Point Cloud Library (PCL), presented in chapter 2, API interface compatible with the software programming language Python.

Table 4.8: Tree and shrub characterisation.

Case study	Plot area [m^2]	Tree measurement			Shrub measurements	
		Tree density [trees/m^2]	Max. tree height [m]	Mean DBH [cm]	Average shrub height [m]	Shrub total cover [%]
PC	3529	0.006	20.4	51.7	1.50	3
CG	1168	0.02	33.4	44.6	–	–
SECIL1	200	0.19	8.5	12.7	1.00	27
SECIL2	200	0.18	10.8	14.8	1.70	67
SECIL3	200	–	–	–	0.60	44
SECIL4	200	0.09	12.0	23.78	0.58	71

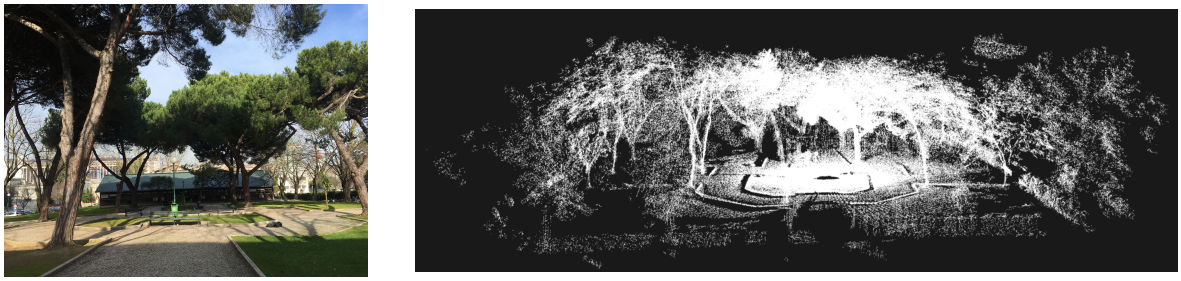

(a) (b)

Figure 4.5: Photograph (a) and point cloud data (b) of the studied plot at PC.

(a) (b)

Figure 4.6: Photograph (a) and point cloud data (b) of the studied plot at CG.

(a)

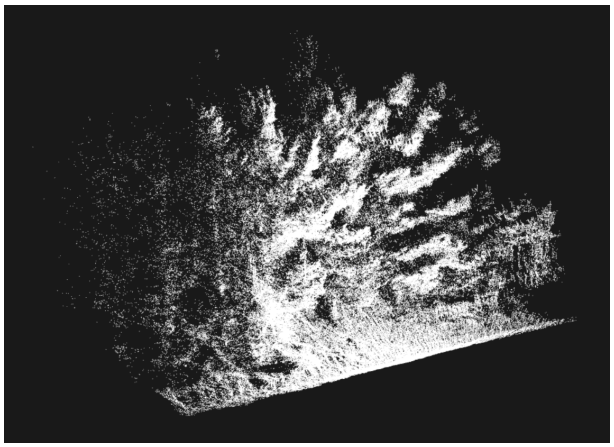

(b)

Figure 4.7: Photograph (a) and point cloud data (b) of the studied plot at SECIL1.

(a)

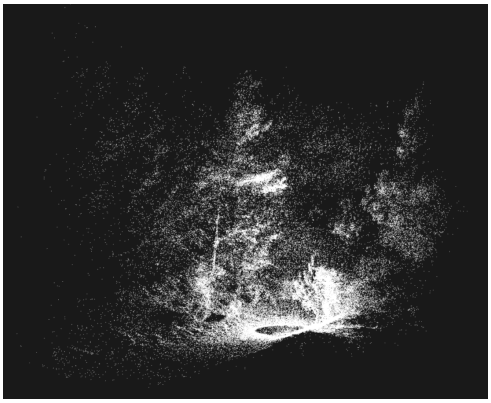

(b)

Figure 4.8: Photograph (a) and point cloud data (b) of the studied plot at SECIL2.

(a)

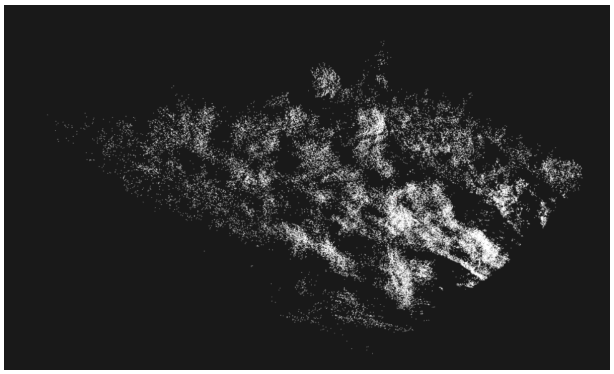

(b)

Figure 4.9: Photograph (a) and point cloud data (b) of the studied plot at SECIL3.

4.4.3 Histograms of vegetation structure

Histograms of vegetation structure represent the variation of the number of points according to their height to ground, which are a proxy for leaf density. The first step to create these histograms is to filter all duplicate points, which can be done using the function filter_duplicate from lidR package [29, 30], a R package for ALS data processing. This function excludes points with identical XYZ coordinates, as

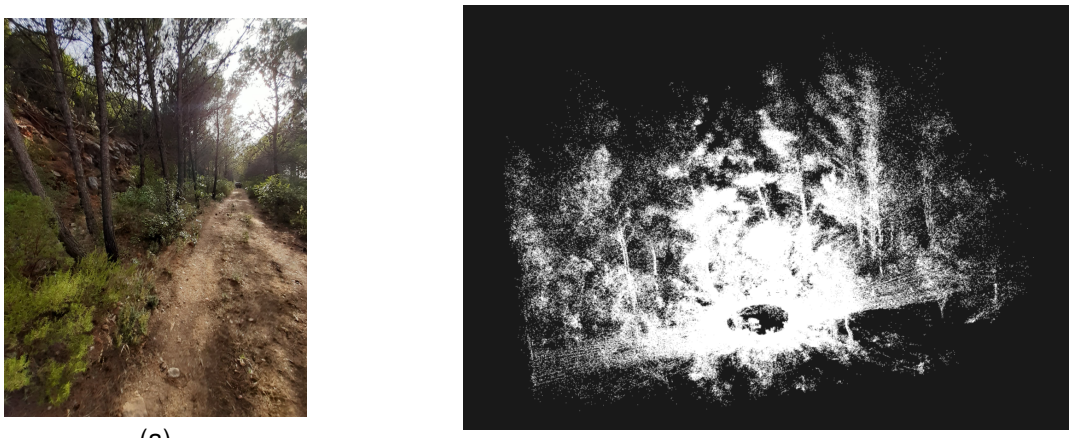

(a) (b)

Figure 4.10: Photograph (a) and point cloud data (b) of the studied plot at SECIL4.

they represent the same object and can give false idea of changes in leaf density. Height to ground of each points can be calculated using an overlapping digital terrain model (DTM) of the studied area and the function normalize_height, also from the lidR package. DTM of each location was computed using the tool las2dem from the LAStools [24] application. The calculated heights can then be represented as a histogram using the function ggplot, from the ggplot2 [42] R package. Figure 4.11 presents these results for each location. These histograms represent number of points as percentage of total number of points in height intervals of 20cm, starting at 20cm above ground. The interval 0cm-20cm is excluded since it holds the largest amount of points due to ground returns, which would decrease visualisation of the other height ranges, corresponding to the actual vegetation.

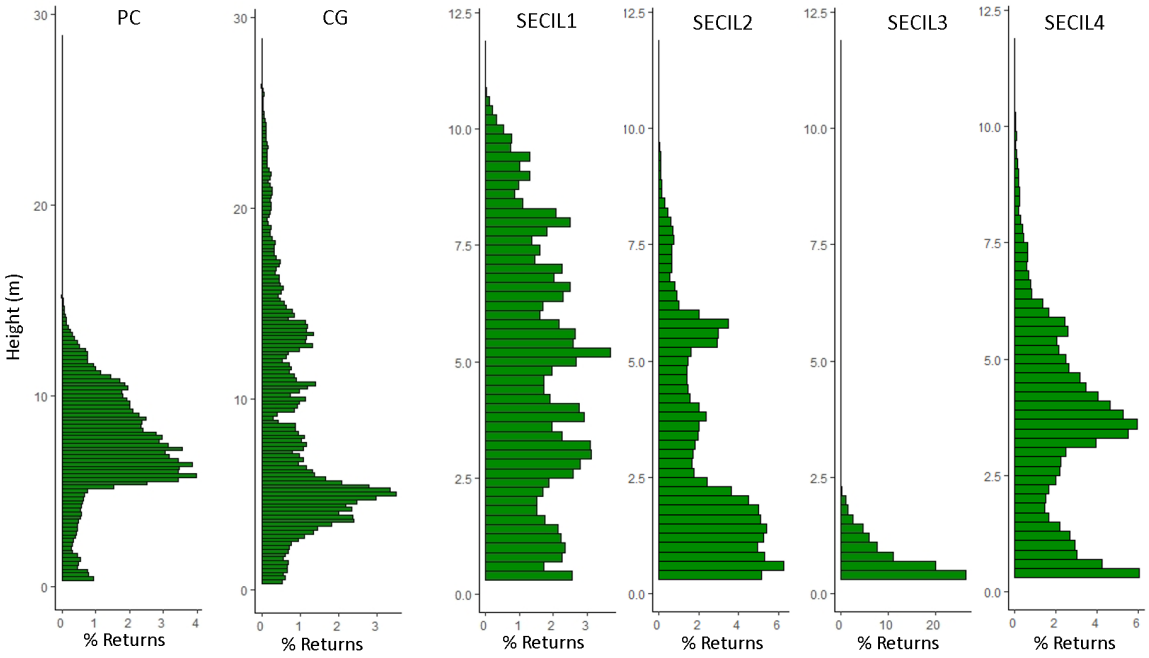

Figure 4.11: Histogram of vegetation structure for each studied location.

The resulting histograms of vegetation clearly show differences observed in field measurements.

Looking at the vegetation structure histograms (Figure 4.11), point cloud data allowed to distinguish two main vegetation structures of the environment, the shrub and tree layers, separated by a minimum percentage of returns, which represent an horizontal layer mostly containing three trunks and showing minimum leaf density. Both urban gardens show highest trees with maximum values surpassing 15m in PC and 25m in CG. Furthermore, its also possible to confirm that returns are minimum for lower heights, reflecting a poorly developed or absent shrub stratum, when compared to that of trees. In what concerns the SECIL quarry plots, the absence of tree stratum in SECIL3 is clearly visible in the absent number of returns at heights above 2.5m. In addition, the large size of shrubes in SECIL2 is also visible in the percentage of returns at heights lower than 2.5m. The highest percentage of returns above the 2.5m height in SECIL4 reflects the largest tree size (and consequently canopy size and leaf density), reflected in the largest average DBH measured in the field (Table 4.8).

4.4.4 Vegetation structural index

The diversity of vegetation height classification was calculated using the Shannon index, which is the most common diversity index applied to heights in LiDAR studies in ecology [9–11], which numerically represent the vegetation complexity in the vertical stratum for specific class of heights (here, 50cm height classes were used). The Shannon index was determined using the diversity function from vegan [43], a R package which provides tools for basic diversity analyses, community ordination and dissimilarity analysis. The Shannon index, H, is determined through the expression (4.2), where p_i is the proportion of total sample represented by height class i. Table 4.9 shows results obtained for the Shannon index in each location.

$$H = -\sum p_i \times ln(p_i) \tag{4.2}$$

Table 4.9: Shannon index for each sampled location.

Case studies	Shannon index
PC	3.04
CG	3.61
SECIL1	2.95
SECIL2	2.59
SECIL3	0.94
SECIL4	2.62

Shannon diversity index is a quantitative measurement that reflects the diversity of vegetation with different height structure, where taller vegetation structures will have larger height diversity. Amongst the urban parks, CG has the highest vegetation structural diversity than PC. Between SECIL plots, SECIL1 shows highest structural diversity and SECIL3 is the opposite, showing lower diversity. Overall, the shrub cover detected in the field is comparable with the proportion of shrubs returns calculated with the LiDAR system.

4.4.5 Point cloud data comparison with field data

To serve as comparison between point cloud data and field data, for each location, maximum height, shrub total cover, height cut-off and returns were determined based on point cloud data. Shrub height cut-off corresponds to the estimated maximum height of shrubs retrieved from the vegetation height histograms, which also corresponds to a minimum percentage return in middle of the histogram, separating shrub from tree stratum (Figure 4.11). Shrub return is an estimation of shrub cover calculated from point cloud data. This estimation is calculated using expression (4.3), where NSR is the number of shrub returns, NSP the number of shrub points and NGP is the number of ground points. Table 4.10 presents these measurements for each locations.

$$NSR = \frac{NSP}{NSP + NGP} \tag{4.3}$$

Table 4.10: Environment characterisation using point cloud data. NGP is the number of ground points, NSP is the number of shrub points, NSR is the number of shrub returns.

Case studies	Max. height [m]	Shrub height cut-off [m]	NGP	NSP	NSR [%]
PC	17.09	1.5	394638	41410	1
CG	28.01	–	–	–	–
SECIL1	11.34	2	34622	138194	28
SECIL2	10.75	2.5	290198	400656	58
SECIL3	–	2.5	104003	45337	43.60
SECIL4	11.47	2	224888	217006	49

For the urban gardens, PC and CG, maximum tree height in Table 4.10 are greatly underestimated those from 4.8, up to difference of 5.39m, while for the locations at SECIL, although also underestimated, have a difference up to 0.53m. This variation is due to vegetation density of tree canopy, which can produce great level of occlusion.

Summarising, field observations agree well with graphical representations of the point cloud (Figure 4.11) and with the structural diversity index applied. This shows that the developed LiDAR system can detect changes in the vegetation structure, even in areas with high vegetation density.

4.5 MLS system comparison

For further assessment, the acquired data from the developed LiDAR system was also compared with data acquired by a VUX LiDAR system. VUX is a MLS type system, developed by Albatroz Engenharia SA. [44], which performs data acquisitions in the vertical plane along an oblique line (Figure 4.12) while in constant movement for point acquisition of great areas. The sensor used in this implementation is RIEGL's VUX-1UAV [45], a waveform LiDAR designed to meet measurement performance and integration requirements of ALS. This sensor provides high speed data acquisition using solely one narrow laser beam, compromising to a field of view of 330° over one plane. Measurement rate is up to 500000 per second, with a maximum range of 1050 m, dependent on laser pulse repetition rate (see Table 4.11 for more details on sensor specifications). This sensor was implemented in order to acquire oblique lines

in the vertical plane. This method allows to change the observation method of vegetation, increasing its characterisation (Figure 4.13).

Table 4.11: RIEGL VUX-1UAV sensor specifications, adapted from the datasheet provided by the manufacturer.

Laser pulse repetition rate	50 kHz	100 kHz	200 kHz	300 kHz	380 kHz	550 kHz	
Maximum range[1]	1050 m	760 m	550 m	450 m	400 m	340 m	170 m
Maximum operating flight altitude[2]	590 m	420 m	310 m	260 m	230 m	190 m	100 m
Maximum number of targets per pulse	15	15	13	9	7	4	4
Minimum range	3 m						
Accuracy	10 mm						
Field of view (horizontal)	330°						
Laser wavelength	near infrared						
Rotation speed	10 - 200 revelations per second						
Operating voltage	11 - 34 V						
Communication interface	LAN						

[1] typical values for average conditions 80% lase reflectively.
[2] typical values for 60% laser reflectively.
[3] flat terrain assumed, scan angle ±45° FOV.

Figure 4.12: MLS implementation using RIEGL VUX-1UAV LiDAR sensor.

4.5.1 Case studies

This system was used to acquire point cloud data at the limestone quarry mentioned previously (Figure 4.4). From the area accessed by this system, only three locations were acquired by VUX and LCLS: SECIL1, SECIL2 and SECIL3. Figures 4.14, 4.15 and 4.16 show the visualisation of the studied plot area for each location common with LCLS.

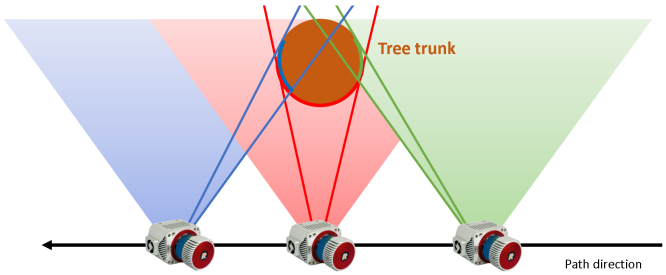

Figure 4.13: Conceptual performance in acquiring data about a tree trunk using oblique lines in the vertical plane with the sensor moving in a straight path.

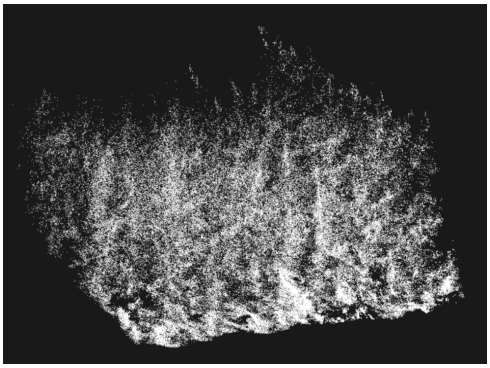

Figure 4.14: Point cloud of VUX MLS at SECIL1.

4.5.2 Histograms of vegetation structure

VUX point cloud data was also used to compute histograms of vegetation structure. These histograms used the same method as the histograms computed for LCLS data. Figure 4.17 presents the histograms data of both VUX and LCLS for each common location.

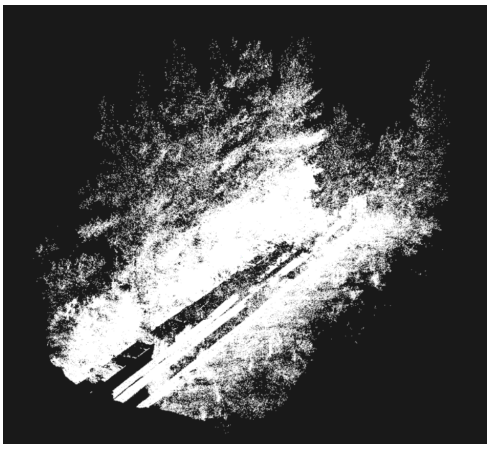

Figure 4.15: Point cloud of VUX MLS at SECIL2.

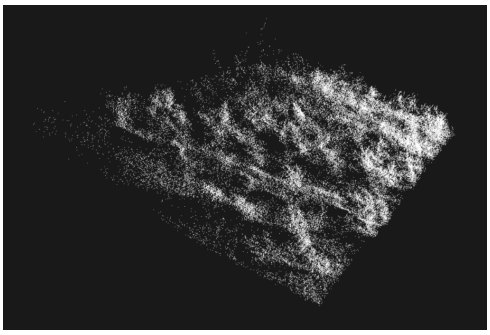

Figure 4.16: Point cloud of VUX MLS at SECIL3.

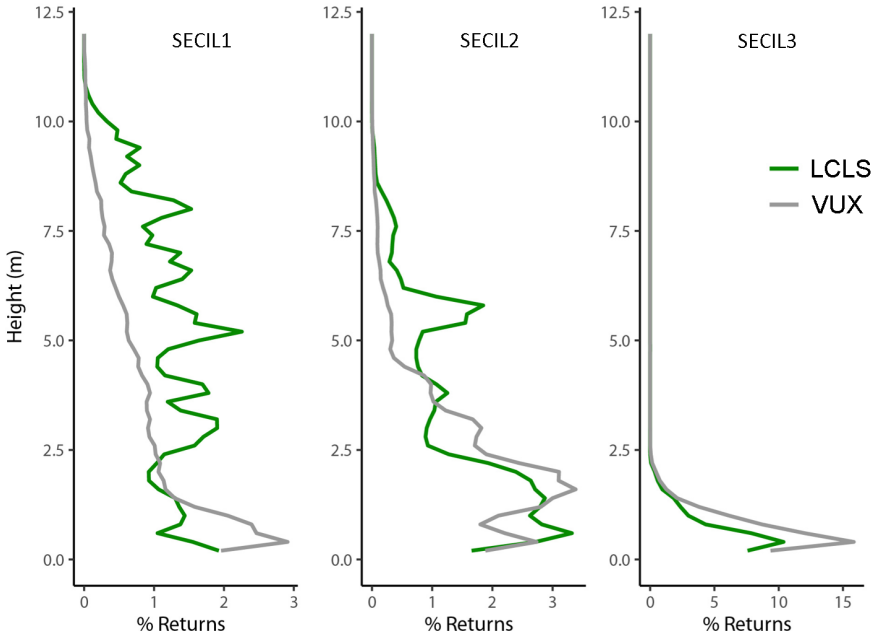

Figure 4.17: Histogram of vegetation structure of both VUX and VLP data for SECIL1, SECIL2 and SECIL3 locations.

4.5.3 Point density

After clipping point cloud data from both VUX and LCLS data according to the field plots, point density for each the locations SECIL1, SECIL2 and SECIL3 were computed using the function grid_density from lidR package. Using ArcMap v.10.6.1 (ESRI, 2019) point density was presented as number of points per grid cells of size 1m for each location.

Looking at the results in the Figure 4.18, it's clear that both system acquire more detailed information in areas closer to the sensor. From the results of LCLS, point density varies from the position of system in a circular pattern, with highest values being closest to the centre and decreasing with distance. This results were expected since LCLS is a stationary system. For VUX, which is a mobile system, the results show a more uniform variation of point density where point density was always highest in regions closest to the path taken by the system, although not has high compared to LCLS, and decreasing with distance to path. LCLS shows a more advantageous instrument for acquisition of distances closer to the sensor, achieving a point density surpassing 50000 points/m^2.

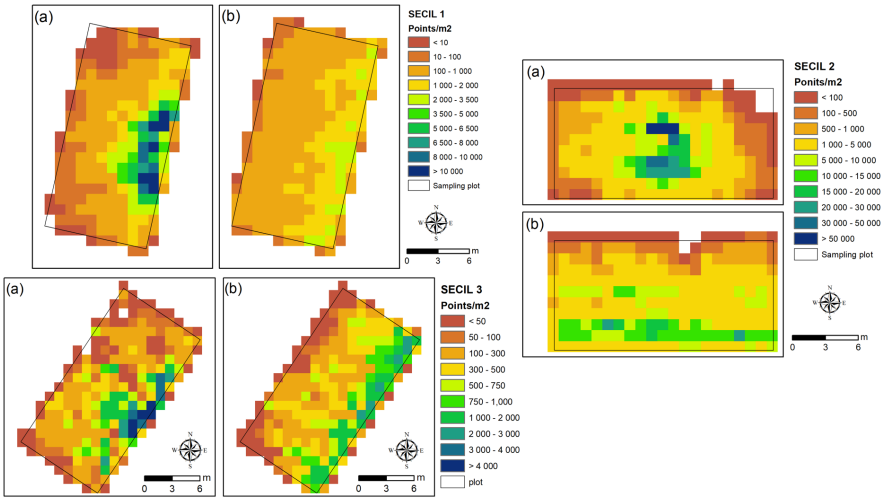

Figure 4.18: Point density representation for the locations SECIL1, SECIL2 and SECIL3. LCLS point cloud data corresponds to (a) and VUX point cloud data corresponds to (b).

4.5.4 Point cloud data comparison with VUX data

By observing the previous results, the developed LiDAR system was capable of detecting higher detail in vegetation structure with the tallest trees. The VUX system loses information in height, which shows the importance of the sensor location in mobile acquisitions. This system was not reaching the same 360° vertical plane acquisition as LCLS, which mostly likely was caused by occlusion effects when acquiring data from different positions of observation. For vegetation structures with lower height (such as as 2.5m shrubs height from SECIL3) both LCLS and VUX showed similar results. Point density was higher for LCLS acquisition, with higher densities near the sensor. VUX had lower point density, which is expected since movement of the LiDAR sensor translates to decreased standing time for data acquisition [13].

4.6 Requirement evaluation

Previously, in chapter 3, six requirements were listed: High accuracy and resolution, Digital modelling of vegetation, Open data format, Provide useful data, Low cost and Ease of use. From the various tests performed, LCLS managed to positively respond to each one of the these requirements. Accuracy and resolution evaluation is described in section 4.2. Digital modelling of vegetation was evaluated by determining the quality of point cloud digital reconstruction. Resulting point clouds were saved in txt file formats, one of the most common formats (see section 2.2.3), from which the software applications and tools used easily read and allow conversion to more appropriate formats. In sections 4.3 is presented how environment classification can acquired with the use of point cloud data, which proved useful, serving as a great complement to field data. Although the total system cost exceeded the specified threshold of 10000€, due to cost of the LiDAR sensor (see section 4.1), with the implementation of cheaper LiDAR sensors, similar results presented in this work may be acquired. Ease of use was evaluated by determining how easy is for the user to mount the system, which equated to around 5 minutes.

Chapter 5

Conclusion and future work

This thesis only briefly showed the utility of LiDAR systems in plant ecology studies. These systems are widely used with continuous improvements, however, commercially available options are expensive with limited software support for ecology studies, leaving specialists to develop their own applications. As such, the objective of this work was to develop the presented LCLS. This system had to follow several requirements, with the main focus being on developing a stationary LiDAR system with a total price below 10000€.

The main idea of the developed system was to change the orientation of a LiDAR sensor, that was capable of acquiring data with a horizontal field of view of 360°, in order to acquire distance measurements in a vertical plane. With complementary add-nos, such as a turn table and a step motor, sensors, such as an accelerometer, a gyroscope and a magnetometer, and a GPS, field of view of the LiDAR sensor was increased and allowed automation of point cloud correction and georeferencing. Although, due to cost the LiDAR sensor used, the developed LCLS had a total cost above the the stipulated value, there are many options of cheaper LiDAR sensors in the market with similar measurements specifications, which would allow to greatly reduce the system's cost.

The system was tested in two types of environments, controlled and field tests. During performance analysis in the controlled environment, LCLS shown highly accurate distance measurements and point cloud resolution, acceptable accuracy in tilt calculations and some problems in determining angle difference with north, which may be caused due to calibration of the sensors used for comparison. After acquiring point cloud data during field tests, histograms of vegetation structure, represented as variation of percentage of total points from point cloud per ground height range, and the Shannon diversity index were computed which provided great insight in the environment vegetation complexity, complementing field measurements. When compared with a MLS, LCLS was considered the most appropriate tool for designated plot area. For acquisitions of larger areas the suggested system would be MLS.

In conclusion, LCLS showed promising results, having achieved the most important requirements. However, many improvements can be made, i.e. better sensor configuration and calibration methods, allow acquisition of multiple position within a plot area to form a point cloud with increased structure characterisation, and integration of RGB cameras with point cloud, which could used improve point

classification (ground, non-ground, vegetation). For future work, it may also be interesting to develop a low cost mobile system, with similar requirements, in order to further increase the use of remote sensing technology in ecology studies.

Bibliography

[1] P. Aplin. Remote sensing: ecology. *Progress in Physical Geography*, 29(1):104–113, 2005.

[2] J. Roughgarden, S. W. Running, and P. A. Matson. What does remote sensing do for ecology? *Ecology*, 72(6):1918–1922, 1991.

[3] K. Wang, S. E. Franklin, X. Guo, and M. Cattet. Remote sensing of ecology, biodiversity and conservation: a review from the perspective of remote sensing specialists. *Sensors*, 10(11):9647–9667, 2010.

[4] K. Lim, P. Treitz, M. Wulder, B. St-Onge, and M. Flood. Lidar remote sensing of forest structure. *Progress in physical geography*, 27(1):88–106, 2003.

[5] M. Dassot, T. Constant, and M. Fournier. The use of terrestrial lidar technology in forest science: application fields, benefits and challenges. *Annals of forest science*, 68(5):959–974, 2011.

[6] M. Disney. Terrestrial li dar: a three-dimensional revolution in how we look at trees. *New Phytologist*, 222(4):1736–1741, 2019.

[7] D. R. A. d. Almeida, S. C. Stark, R. Chazdon, B. W. Nelson, R. G. César, P. Meli, E. Gorgens, M. M. Duarte, R. Valbuena, V. S. Moreno, et al. The effectiveness of lidar remote sensing for monitoring forest cover attributes and landscape restoration. *Forest Ecology and Management*, 438:34–43, 2019.

[8] C. Edson and M. G. Wing. Airborne light detection and ranging (lidar) for individual tree stem location, height, and biomass measurements. *Remote Sensing*, 3(11):2494–2528, 2011.

[9] C. M. Listopad, M. Köbel, A. Príncipe, P. Gonçalves, and C. Branquinho. The effect of grazing exclusion over time on structure, biodiversity, and regeneration of high nature value farmland ecosystems in europe. *Science of the Total Environment*, 610:926–936, 2018.

[10] C. M. Listopad, R. E. Masters, J. Drake, J. Weishampel, and C. Branquinho. Structural diversity indices based on airborne lidar as ecological indicators for managing highly dynamic landscapes. *Ecological Indicators*, 57:268–279, 2015.

[11] J. T. Fisher, B. F. Erasmus, E. T. Witkowski, J. van Aardt, K. J. Wessels, and G. P. Asner. Savanna woody vegetation classification–now in 3-d. *Applied Vegetation Science*, 17(1):172–184, 2014.

[12] M. Melin, A. Shapiro, and P. Glover-Kapfer. Lidar for ecology and conservation - wwf conservation technology series (3). 10 2017. doi: 10.13140/RG.2.2.22352.76801.

[13] M. Beland, G. Parker, B. Sparrow, D. Harding, L. Chasmer, S. Phinn, A. Antonarakis, and A. Strahler. On promoting the use of lidar systems in forest ecosystem research. *Forest Ecology and Management*, 450:117484, 2019.

[14] M. Bosse, R. Zlot, and P. Flick. Zebedee: Design of a spring-mounted 3-d range sensor with application to mobile mapping. *IEEE Transactions on Robotics*, 28:1104–1119, 10 2012. doi: 10.1109/TRO.2012.2200990.

[15] W. Linder. *Digital photogrammetry*, volume 1. Springer, 2009.

[16] G. A. Shaw and H. K. Burke. Spectral imaging for remote sensing. *Lincoln laboratory journal*, 14 (1):3–28, 2003.

[17] J.-B. Féret and G. P. Asner. Tree species discrimination in tropical forests using airborne imaging spectroscopy. *IEEE Transactions on Geoscience and Remote Sensing*, 51(1):73–84, 2012.

[18] M. P. Ferreira, M. Zortea, D. C. Zanotta, Y. E. Shimabukuro, and C. R. de Souza Filho. Mapping tree species in tropical seasonal semi-deciduous forests with hyperspectral and multispectral data. *Remote Sensing of Environment*, 179:66–78, 2016.

[19] A. L. Gil, L. Núñez-Casillas, M. Isenburg, A. A. Benito, J. J. R. Bello, and M. Arbelo. A comparison between lidar and photogrammetry digital terrain models in a forest area on tenerife island. *Canadian Journal of Remote Sensing*, 39(5):396–409, 2013.

[20] J. O. Sexton, T. Bax, P. Siqueira, J. J. Swenson, and S. Hensley. A comparison of lidar, radar, and field measurements of canopy height in pine and hardwood forests of southeastern north america. *Forest Ecology and Management*, 257(3):1136–1147, 2009.

[21] M. J. Sumnall, R. A. Hill, and S. A. Hinsley. Comparison of small-footprint discrete return and full waveform airborne lidar data for estimating multiple forest variables. *Remote Sensing of Environment*, 173:214–223, 2016.

[22] D. S. Hall. High definition lidar system, July 1 2014. US Patent 8,767,190.

[23] F. Pirotti. Open software and standards in the realm of laser scanning technology. *Open Geospatial Data, Software and Standards*, 4(1):14, 2019.

[24] C. Hug, P. Krzystek, and W. Fuchs. Advanced lidar data processing with lastools. In *XXth ISPRS Congress*, pages 12–23, 2004.

[25] R. Mcgaughey. Fusion/ldv: Software for lidar data analysis and visualization - v3.10. *USDA Forest Service*, 01 2014.

[26] L. M. Scott and M. V. Janikas. Spatial statistics in arcgis. In *Handbook of applied spatial analysis*, pages 27–41. Springer, 2010.

[27] J. E. McKendry and J. R. Eastman. Applications of gis in forestry: a review, 1991.

[28] A. Lau, L. P. Bentley, C. Martius, A. Shenkin, H. Bartholomeus, P. Raumonen, Y. Malhi, T. Jackson, and M. Herold. Quantifying branch architecture of tropical trees using terrestrial lidar and 3d modelling. *Trees*, 32(5):1219–1231, 2018.

[29] J.-R. Roussel, D. Auty, F. De Boissieu, and A. Meador. lidr: Airborne lidar data manipulation and visualization for forestry applications. *R package version*, 1(1), 2018.

[30] J.-R. Roussel, D. Auty, N. C. Coops, P. Tompalski, T. R. Goodbody, A. S. Meador, J.-F. Bourdon, F. de Boissieu, and A. Achim. lidr: An r package for analysis of airborne laser scanning (als) data. *Remote Sensing of Environment*, 251:112061, 2020. ISSN 0034-4257. doi: https://doi.org/10.1016/j.rse.2020.112061. URL http://www.sciencedirect.com/science/article/pii/S0034425720304314.

[31] R. B. Rusu and S. Cousins. 3d is here: Point cloud library (pcl). In *2011 IEEE International Conference on Robotics and Automation*, pages 1–4, 2011. doi: 10.1109/ICRA.2011.5980567.

[32] circuito.io: https://www.instructables.com/automated-turntable-with-steppermotor/, accessed on 16 February 2020.

[33] Nema 17hs13-0404s1: https://www.ptrobotics.com/motor-stepper/5782-nema-17-bipolar-18deg-26ncm-368ozin-04a-12v-42x42x34mm-4-wires.html, accessed on 21 February 2020.

[34] Pololu tic t500: https://www.ptrobotics.com/pontes-h/5982-tic-t500-usb-multi-interface-stepper-motor-controller.html, accessed on 21 February 2020.

[35] Sparkfun lsm6ds3: https://www.ptrobotics.com/imu/5367-sparkfun-6-degrees-of-freedom-breakout-lsm6ds3.html, accessed on 5 August 2020.

[36] Gy-511 lsm303dlhc: https://www.ptrobotics.com/acelerometros/7207-gy-511-lsm303dlhc-compass-3-axis-accelerometer-and-magnetometer-sensor-module.html, accessed on 5 August 2020.

[37] B. McCarron. Low-cost imu implementation via sensor fusion algorithms in the arduino environment. 2013.

[38] D. Girardeau-Montaut. Cloudcompare, 2016.

[39] A. Manos, I. Klein, and T. Hazan. Gravity-based methods for heading computation in pedestrian dead reckoning. *Sensors*, 19(5):1170, 2019.

[40] R. H. Canfield. Application of the line interception method in sampling range vegetation. *Journal of forestry*, 39(4):388–394, 1941.

[41] Python-pcl: https://github.com/strawlab/python-pcl, accessed on 18 February 2020.

[42] H. Wickham. ggplot2. *Wiley Interdisciplinary Reviews: Computational Statistics*, 3(2):180–185, 2011.

[43] J. Oksanen, F. G. Blanchet, M. Friendly, R. Kindt, P. Legendre, D. McGlinn, P. R. Minchin, R. O'hara, G. L. Simpson, P. Solymos, et al. vegan: Community ecology package. r package version 2.4-3. 2016.

[44] Albatroz engenharia sa.: https://www.albatroz-eng.com/, accessed on 20 December 2020.

[45] RIEGL. Vux-1uav lidar model: http://www.riegl.com/products/unmanned-scanning/riegl-vux-1uav/, accessed on 20 December 2020.

Appendix A

Annex

Figure A.1 shows the certificate of participation at a meeting of ecologists, XIX National Ecology Meeting organised by SPECO (Portuguese Ecology Society).

Figure A.1: Certificate of participation at a meeting of ecologists